IEEE Access
Multidisciplinary ⋮ Rapid Review ⋮ Open Access Journal

Received 28 June 2024, accepted 17 July 2024, date of publication 24 July 2024, date of current version 1 August 2024.

*Digital Object Identifier 10.1109/ACCESS.2024.3432868*

RESEARCH ARTICLE

# Co-Design of USV Control System Based on Fuzzy Satisfactory Optimization for Automatic Target Arriving and Berthing

**TAOYI CHEN[1,2], HUIXIANG PENG[1,2], XIAOYU CHANG[1,2], XIAONAN ZHANG[1,2], AND DIDI WANG[3]**

[1]The 54th Research Institute of China Electronics Technology Group Corporation, Shijiazhuang 050081, China
[2]CETC Key Laboratory of Aerospace Information Applications, Shijiazhuang 050081, China
[3]School of Electrical and Information Engineering, Tianjin University, Tianjin 300072, China

Corresponding author: Didi Wang (tju_ddw_0720@163.com)

**ABSTRACT** Most of the previous research about unmanned surface vehicle (USV) control system just focuses on reaching the target but not considers berthing. Moreover, computation cost is rarely concerned. For automatic target arriving and berthing of USV in presence of multi-shape convex obstacles and disturbances, this paper designs a composite control system including trajectory optimization and trajectory tracking. In order to generate a smooth and optimal trajectory, two objectives including minimum running time and energy consumption are proposed, and their priority requirement is presented. Fuzzy satisfactory optimization is introduced to reformulate the objective functions, and the membership degree difference is used to model priority between two objectives. The obstacle avoidance constraint is developed based on the improved P-criterion. The comprehensive optimization model is established to obtain the maximum membership degree. Further, the priority optimization model is proposed to expand the feasible domain by relaxing the comprehensive optimization result. Two models are discretized by Gaussian pseudospectral method to find the optimal solution. To achieve good trajectory tracking under disturbances, two first-order active disturbance rejection control (ADRC) controllers are designed to follow the desired longitudinal velocity and course angular velocity. All the velocities of USV can converge. The simulation proves the effectiveness of the proposed co-designed system by comparing with other methods.

**INDEX TERMS** USV, trajectory optimization, trajectory tracking, Gaussian pseudospectral method, ADRC.

## I. INTRODUCTION

Recently, many researchers are engaged in development of unmanned surface vehicle (USV) due to its broad military and civil application prospects. For USV, it is a challenge to reach the desired target position automatically and berth instantly. Most of the research focuses on path or trajectory tracking, however, berthing at the target cannot be guaranteed simultaneously. Therefore, establishment of a composite control system including trajectory optimization and trajectory tracking to complete automatic target arriving and berthing has become a potential issue for USV [1], [2].

Trajectory optimization is a core module for autonomous navigation of USV. Its goal is to generate a smooth, safe, and feasible trajectory. However, the kinematics and dynamics models of USV are nonlinear and differential so that it is difficult for solution [3]. Many methods have been attempted, for example, deep reinforcement learning [4], rapidly-exploring random tree [5], genetic algorithm [6], and gradient algorithm [7]. In addition, it is common to perform a single-objective trajectory optimization. Mills et al. propose the method via the least amount of energy to effectively navigate to a goal point [8]. Wang et al. obtain the total sailing time of USV by making a time-optimal maneuvering [9]. However, single-objective trajectory optimization fails to deal with various performance requirements. Therefore, multi-objective

The associate editor coordinating the review of this manuscript and approving it for publication was Yilun Shang.

optimization is applied to USV, and the weighted strategy becomes the common technique. Kandel et al. use the scalarization weight to deal the tradeoff between fuel consumption and trip time [10]. However, weighted strategy cannot reflect importance of every objective accurately in the case of the non-convex multi-objective optimization.

In addition, accurate trajectory tracking is an essential issue for USV. Generally, the reference trajectory is a time-dependent path. That means that the USV is required to arrive at the waypoints at a specified time. A lot of methods have been attempted, such as backstepping [11], [12], line-of-sight guidance [13], sliding mode control [14], [15], adaptive control [16], and event-triggered method [17]. In reality, arriving at the desired target and berthing there steadily is a common task for USV. However, most research just focuses on reaching the target but not considers berthing. Moreover, disturbances such as wind and waves, have the severe impact on USV's movement control. Besides, USV control is underactuated since only surge force and yaw moments can be used to control more motion states. Some methods are attempted [18], [19], [20], but the difficulty and complexity of control system design are greatly increased as well. Thereafter, how to find an effective approach for achieving trajectory tracking of USV is very important.

Motivated by above, a composite control system to accomplish automatic target arriving and berthing is developed for USV in this paper. Fuzzy multi-objective trajectory optimization is taken as the outer loop and trajectory tracking as the inner loop. The kinematics and dynamics models are both involved in trajectory optimization. The multi-objective trajectory optimization (MTO) with two objectives and priority is formulated, and fuzzy satisfactory optimization idea [21] is introduced. The comprehensive optimization model and priority optimization model are built respectively by relaxing the maximum membership degree and incorporating fuzzy membership degree difference constraint. Wherein, various constraints are involved, and the improved P-criterion obstacle avoidance constraint is designed for multi-shape convex obstacles. Since these two optimization models are continuous and differential equations, Gaussian pseudospectral method is incorporated for discretization at Legendre Gaussian (LG) points. In trajectory tracking in presence of disturbances, two tracking controllers based on active disturbance rejection control (ADRC) are designed to steer the longitudinal velocity and course angular velocity of USV. Then, the trajectory tracking and berthing of USV in presence of obstacles and disturbances can be achieved.

The main contributions of this paper are summarized as follows:

a) A composite control system for automatic target arriving and berthing of USV is developed to reduce feedback cost and facilitate controller design. The constraint of control variables is addressed in trajectory optimization, so the control saturation does not need to be taken into account during controller design.

b) To obtain the optimal reference trajectory in presence of obstacles, the minimum running time and energy consumption are proposed such that multi-objective optimization with priority is formulated. To optimize these objectives fully and satisfy priority requirement, fuzzy satisfactory optimization is followed and fuzzy membership degree difference constraint is presented to handle priority. Accordingly, the comprehensive optimization model and priority optimization model are formulated to realize tradeoff between optimization and priority by relaxing the maximum membership degree. The P-criterion is improved to establish the multi-shape convex obstacle avoidance constraint.

c) To follow the desired longitudinal velocity and course angular velocity accurately under external disturbances, two first-order linear ADRC controllers are developed. Inspite of USV being underactuated, the composite system can still guarantee convergence of transverse velocity by including the dynamics constraint in trajectory optimization.

The paper is structured as follows. Section II interprets the target arriving and berthing task of USV and presents the models. Section III describes the co-design methodology of trajectory optimization and trajectory tracking. The simulation is implemented in Section IV. The conclusions of the paper are drawn in Section V.

## II. PROBLEM DESCRIPTION

### A. TASK DESCRIPTION

In this paper, automatic target arriving and berthing of USV is addressed when multi-shape convex obstacles and disturbances exist, as shown in Figure 1. USV departs from the specific position and moves along the trajectory. Finally it arrives at the target point and berths there. That is, USV needs to compute an optimal trajectory under various constraints and obstacles. The terminal longitudinal velocity, transverse velocity, and course angular velocity at the target point should be zero.

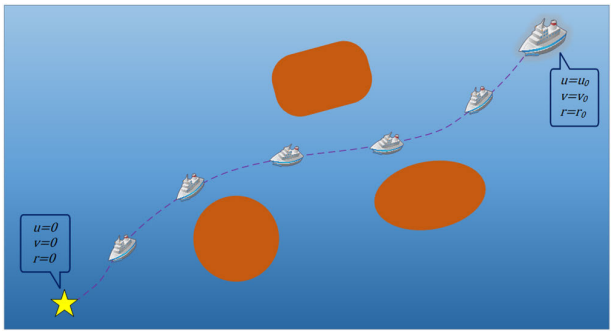


**FIGURE 1.** The schematic of automatic target arriving and berthing.

### B. KINEMATICS MODEL

The three-degree-of-freedom motion with longitudinal, transverse, and bow-swing is concerned in this paper. The

kinematics model of USV is presented as

$$\begin{cases} \dot{x} = u\cos\varphi - v\sin\varphi \\ \dot{y} = u\sin\varphi + v\cos\varphi \\ \dot{\varphi} = r \end{cases} \tag{1}$$

where $x, y, \varphi$ indicate the position and course angle of USV. $u, v, r$ represent the longitudinal velocity, transverse velocity, and course angular velocity respectively.

### C. DYNAMICS MODEL

Assuming that the USV is symmetry, then its dynamics equation is described as

$$\boldsymbol{M}\dot{\boldsymbol{J}} + \boldsymbol{C}\boldsymbol{J} + \boldsymbol{D}\boldsymbol{J} = \boldsymbol{\tau} + \boldsymbol{\tau_d} \tag{2}$$

where $\boldsymbol{J} = [u, v, r]^T$. $\boldsymbol{\tau} = [\tau_u, 0, \tau_r]^T$ indicate surge force and yaw moments. $\boldsymbol{\tau_d} = [d_X, d_Y, d_N]^T$ mean the external disturbances caused by wind and waves. $M, C, D$ represent the inertial matrix, Coriolis matrix, and hydrodynamic damping matrix respectively.

$$\boldsymbol{M} = \begin{bmatrix} m_{11} & 0 & 0 \\ 0 & m_{22} & 0 \\ 0 & 0 & m_{33} \end{bmatrix}, \boldsymbol{D} = \begin{bmatrix} d_{11} & 0 & 0 \\ 0 & d_{22} & 0 \\ 0 & 0 & d_{33} \end{bmatrix} \tag{3}$$

$$\boldsymbol{C} = \begin{bmatrix} 0 & 0 & -m_{22}v \\ 0 & 0 & m_{11}u \\ m_{22}v & -m_{11}u & 0 \end{bmatrix} \tag{4}$$

Then, the dynamics model of USV can be expressed as

$$\begin{cases} \dot{u} = \dfrac{m_{22}}{m_{11}}vr - \dfrac{d_{11}}{m_{11}}u + \dfrac{1}{m_{11}}\tau_u + \dfrac{d_X}{m_{11}} \\ \dot{v} = -\dfrac{m_{11}}{m_{22}}ur - \dfrac{d_{22}}{m_{22}}v + \dfrac{d_Y}{m_{22}} \\ \dot{r} = \dfrac{m_{11} - m_{22}}{m_{33}}uv - \dfrac{d_{33}}{m_{33}}r + \dfrac{1}{m_{33}}\tau_r + \dfrac{d_N}{m_{33}} \end{cases} \tag{5}$$

## III. CO-DESIGN OF USV CONTROL SYSTEM

### A. OVERALL CONTROL SYSTEM

The USV composite control system is shown in Figure 2. In trajectory optimization, two objectives are proposed and fuzzified. Various constraints are involved. By comprehensive optimization model, the maximum fuzzy membership degree can be obtained. Further, priority optimization model realizes priority difference by relaxing the result of comprehensive optimization. By means of Gaussian pseudospectral method, the two models are discretized and solved to obtain the optimal longitudinal velocity trajectory $u_d$ and optimal course angular velocity trajectory $r_d$. In trajectory tracking, two first-order linear ADRC controllers are designed to follow them under the disturbances.

The system uses trajectory optimization as outer loop and trajectory tracking as inner loop. It can be seen that the position feedback is not used and only the speed signal measurement is necessary in tracking control. This reduces the feedback cost and the complexity of controller design.

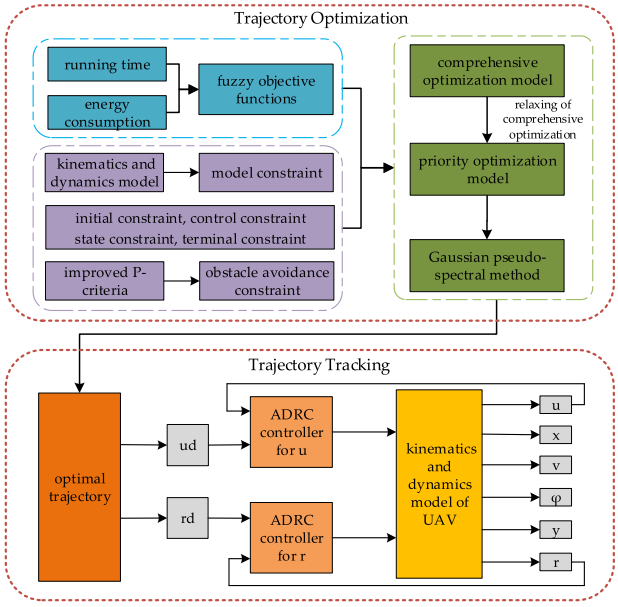


**FIGURE 2.** Schematic of composite USV control system.

Due to the dynamic model constraint, once the longitudinal velocity $u$ and course angular velocity $r$ converge to the desired values, the transverse velocity $v$ will also converge. Thus, $v$ is indirectly stabilized in the underactuated system.

### B. TRAJECTORY OPTIMIZATION

In trajectory optimization, the optimal $u, v, r$ at each waypoint are figured out, and their terminal values are zero.

Firstly, USV is required to arrive at the target as soon as possible. Assuming that USV begins to move at $t_0$ and stops at $t_f$, the running time is presented as follows

$$f_t = t_f - t_0 \tag{6}$$

In addition, less energy consumption is important for USV, and it mainly comes from drag forces. It is known that the rate of energy consumption can be formulated by power, i.e. $P = FV$. $P$ is power, $F$ is drag force, and $V$ is the overall velocity [22]. Drag force $F = k_1 V^2$, and $k_1$ is a constant. The overall velocity is expressed as $V = \sqrt{u^2 + (k_2 r)^2}$, where $k_2$ is the turning radius [10]. Based on the above, a new energy variable $e$ is introduced and its derivative is defined as

$$\dot{e} = (u^2 + (k_2 r)^2)^{\frac{3}{2}} \tag{7}$$

Obviously, $\dot{e}$ can denote the energy consumption rate. Therefore, energy consumption can be formulated as

$$f_e = \int_{t_0}^{t_f} (u^2 + (k_2 r)^2)^{\frac{3}{2}} dt = \int_{t_0}^{t_f} \dot{e} dt = e\left(t_f\right) - e\left(t_0\right) \tag{8}$$

Combined with (1), (5) and (7), the entire model of USV without considering disturbances can be rewritten as

$$\begin{cases} \dot{x} = u\cos\varphi - v\sin\varphi \\ \dot{y} = u\sin\varphi + v\cos\varphi \\ \dot{\varphi} = r \\ \dot{u} = \dfrac{m_{22}}{m_{11}}vr - \dfrac{d_{11}}{m_{11}}u + \dfrac{1}{m_{11}}\tau_u \\ \dot{v} = -\dfrac{m_{11}}{m_{22}}ur - \dfrac{d_{22}}{m_{22}}v \\ \dot{r} = \dfrac{m_{11}-m_{22}}{m_{33}}uv - \dfrac{d_{33}}{m_{33}}r + \dfrac{1}{m_{33}}\tau_r \\ \dot{e} = (u^2 + (k_2 r)^2)^{\frac{3}{2}} \end{cases} \tag{9}$$

Let $\boldsymbol{\xi} = [x, y, \varphi, u, v, r, e]^T$ as the state vector and $\boldsymbol{c} = [\tau_u, \tau_r]^T$ as the control vector. Then, the model constraint can be summarized as

$$\dot{\boldsymbol{\xi}} = g(\boldsymbol{\xi}, \boldsymbol{c}) \tag{10}$$

The state vector of USV needs to satisfy the constraint

$$\boldsymbol{\xi}_{\boldsymbol{min}} \le \boldsymbol{\xi} \le \boldsymbol{\xi}_{\boldsymbol{max}} \tag{11}$$

where $\boldsymbol{\xi}_{\boldsymbol{min}}$ is the minimum of state variables and $\boldsymbol{\xi}_{\boldsymbol{max}}$ is the maximum.

The control vector is limited by the following constraint

$$\boldsymbol{c}_{\boldsymbol{min}} \le \boldsymbol{c} \le \boldsymbol{c}_{\boldsymbol{max}} \tag{12}$$

where $\boldsymbol{c}_{\boldsymbol{min}}$ and $\boldsymbol{c}_{\boldsymbol{max}}$ denote the bounds of control variables.

The initial and terminal conditions of the state vector are respectively

$$\begin{aligned} \boldsymbol{\xi}(t_0) &= \boldsymbol{\xi}_{\mathbf{0}} \\ \boldsymbol{\xi}(t_f) &= \boldsymbol{\xi}_{\boldsymbol{f}} \end{aligned} \tag{13}$$

where $\boldsymbol{\xi}_{\mathbf{0}}$ means the initial states and $\boldsymbol{\xi}_{\boldsymbol{f}}$ represents the terminal states.

In this paper, the multi-shape convex obstacles are concerned, e.g. circles, squares or ellipses, etc. In order to describe obstacles concisely and uniformly, the P-criterion function is often used for modeling obstacle boundary [23]. However, the traditional P-criterion function only focuses on the position of obstacles but not takes their orientation into account. It possibly results in the inaccurate characterization of the obstacle bound. Therefore, the P-criterion function is improved by introducing the orientation as

$$p(x, y) = \left[ \left| \frac{(x-a)\cos\omega + (y-b)\sin\omega}{r_x} \right|^h + \left| \frac{(y-b)\cos\omega + (x-a)\sin\omega}{r_y} \right|^h \right]^{1/h} - 1 \tag{14}$$

where $r_x, r_y$ denote the proportional coefficients in the x-direction and y-direction respectively. $(a, b)$ indicates the coordinates of the obstacle's center. $h$ is the adjustable parameter related to the obstacle shape. And $\omega$ means the angle of obstacle's orientation.

Then the obstacle avoidance constraint is summarized as

$$p(x, y, a_i, b_i, r_{xi}, r_{yi}, \omega_i, h_i) \ge 0, i = 1, \cdots, n \tag{15}$$

where $n$ represents the number of obstacles. The USV is just taken as ideal point in this paper. In reality, the practical obstacle avoidance distance should be bigger due to the sizes of obstacles and USV.

To acquire the optimal trajectory, two objectives including minimum running time and energy consumption are presented. Wherein, how to arrive quickly is the most important. Simultaneously, USV is expected to travel with the smallest energy consumption. The two objectives with priority are presented as

L1 minimum running time: $\min f_t(\boldsymbol{\xi}, \boldsymbol{c}) = t_f - t_0$;

L2 minimum energy consumption: $\min f_e(\boldsymbol{\xi}, \boldsymbol{c}) = e(t_f) - e(t_0)$

As traveling faster will consume more energy, these two goals are conflicting [24]. That is, when the USV travels fast, the short time will be spent and a great deal of energy will be used. Furthermore, two optimization objectives are non-normalized. Therefore, fuzzy satisfaction optimization is introduced to reformulate the two objectives. The fuzzy membership functions are defined as

$$u_t(\boldsymbol{\xi}, \boldsymbol{c}) = \begin{cases} 1, f_t(\boldsymbol{\xi}, \boldsymbol{c}) \le f_t^* \\ 1 - \dfrac{f_t(\boldsymbol{\xi}, \boldsymbol{c}) - f_t^*}{f_t^{\max} - f_t^*}, f_t^* \le f_t(\boldsymbol{\xi}, \boldsymbol{c}) \le f_t^{\max} \\ 0, f_t(\boldsymbol{\xi}, \boldsymbol{c}) \ge f_t^{\max} \end{cases} \tag{16}$$

$$u_e(\boldsymbol{\xi}, \boldsymbol{c}) = \begin{cases} 1, f_e(\boldsymbol{\xi}, \boldsymbol{c}) \le f_e^* \\ 1 - \dfrac{f_e(\boldsymbol{\xi}, \boldsymbol{c}) - f_e^*}{f_e^{\max} - f_e^*}, f_e^* \le f_e(\boldsymbol{\xi}, \boldsymbol{c}) \le f_e^{\max} \\ 0, f_e(\boldsymbol{\xi}, \boldsymbol{c}) \ge f_e^{\max} \end{cases} \tag{17}$$

where $f_t^*, f_e^*$ are the expected values of two objectives, and $f_t^{\max}, f_e^{\max}$ are the maximum. They can be determined using the payoff table in Table 1 through single-objective optimization.

**TABLE 1. Payoff table.**

| | $f_t$ | $f_e$ |
|---|---|---|
| $\min f_t(\xi, c)$ | $f_t(\xi_t, c_t)$ | $f_e(\xi_t, c_t)$ |
| $\min f_e(\xi, c)$ | $f_t(\xi_e, c_e)$ | $f_e(\xi_e, c_e)$ |

$(\boldsymbol{\xi}_{\boldsymbol{t}}, \boldsymbol{c}_{\boldsymbol{t}})$ and $(\boldsymbol{\xi}_{\boldsymbol{e}}, \boldsymbol{c}_{\boldsymbol{e}})$ represent the optimal solutions of single-objective optimization. Accordingly, the fuzzy multi-objective optimization model is presented as follows

$$\begin{aligned} &\max\left[L_1(\mu_t(\boldsymbol{\xi}, \boldsymbol{c})), L_2(\mu_e(\boldsymbol{\xi}, \boldsymbol{c}))\right] \\ &\text{s.t. } \boldsymbol{\xi}_{\boldsymbol{min}} \le \boldsymbol{\xi} \le \boldsymbol{\xi}_{\boldsymbol{max}} \\ &\quad \boldsymbol{c}_{\boldsymbol{min}} \le \boldsymbol{c} \le \boldsymbol{c}_{\boldsymbol{max}} \\ &\quad \boldsymbol{\xi}(t_0) = \boldsymbol{\xi}_{\mathbf{0}} \\ &\quad \boldsymbol{\xi}(t_f) = \boldsymbol{\xi}_{\boldsymbol{f}} \\ &\quad \dot{\boldsymbol{\xi}} = g(\boldsymbol{\xi}, \boldsymbol{c}) \end{aligned}$$

$$
\begin{aligned}
&p\left(\boldsymbol{\xi}(1), \boldsymbol{\xi}(2), a_i, b_i, r_{xi}, r_{yi}, \omega_i, h_i\right) \geq 0, i=1, \cdots, n \\
&u_t(\boldsymbol{\xi}, \boldsymbol{c})=1-\frac{f_t(\boldsymbol{\xi}, \boldsymbol{c})-f_t^*}{f_t^{\max }-f_t^*} \\
&u_e(\boldsymbol{\xi}, \boldsymbol{c})=1-\frac{f_e(\boldsymbol{\xi}, \boldsymbol{c})-f_e^*}{f_e^{\max }-f_e^*}
\end{aligned} \tag{18}
$$

where $L_1, L_2$ represent the priority factors, $\boldsymbol{\xi}(1)$ and $\boldsymbol{\xi}(2)$ mean the first and second elements of $\boldsymbol{\xi}$ respectively.

To ensure the membership degrees being effective, the following inequality is presented

$$
\begin{aligned}
&\alpha \leq \mu_t(\boldsymbol{\xi}, \boldsymbol{c}) \leq 1 \\
&\alpha \leq \mu_e(\boldsymbol{\xi}, \boldsymbol{c}) \leq 1
\end{aligned} \tag{19}
$$

where $\alpha \in (0,1)$. In order to optimize both objectives as much as possible, the first step is to find out the maximum membership degree of these two objectives under relevant constraints. Then, the comprehensive optimization model is proposed as

$$
\begin{cases}
\max \alpha \\
\boldsymbol{\xi_{min}} \leq \boldsymbol{\xi} \leq \boldsymbol{\xi_{max}} \\
\boldsymbol{c_{min}} \leq \boldsymbol{c} \leq \boldsymbol{c_{max}} \\
\boldsymbol{\xi}\left(t_0\right)=\boldsymbol{\xi_0} \\
\boldsymbol{\xi}\left(t_f\right)=\boldsymbol{\xi_f} \\
\dot{\boldsymbol{\xi}}=g(\boldsymbol{\xi}, \boldsymbol{c}) \\
p\left(\boldsymbol{\xi}(1), \boldsymbol{\xi}(2), a_i, b_i, r_{xi}, r_{yi}, \omega_i, h_i\right) \geq 0, i=1, \cdots, n \\
\alpha \leq \mu_t(\boldsymbol{\xi}, \boldsymbol{c}) \leq 1 \\
\alpha \leq \mu_e(\boldsymbol{\xi}, \boldsymbol{c}) \leq 1 \\
u_t(\boldsymbol{\xi}, \boldsymbol{c})=1-\dfrac{f_t(\boldsymbol{\xi}, \boldsymbol{c})-f_t^*}{f_t^{\max }-f_t^*} \\
u_e(\boldsymbol{\xi}, \boldsymbol{c})=1-\dfrac{f_e(\boldsymbol{\xi}, \boldsymbol{c})-f_e^*}{f_e^{\max }-f_e^*}
\end{cases} \tag{20}
$$

Due to the principle that the higher-priority objective has a higher-level satisfaction [21], priority can be expressed through the comparison of membership degrees. Accordingly, priority constraint in this paper can be obtained as

$$
\mu_e(\boldsymbol{\xi}, \boldsymbol{c}) \leq \mu_t(\boldsymbol{\xi}, \boldsymbol{c}) \tag{21}
$$

However, in some cases, the comparison inequality is too strict to ensure optimization feasible. Variable $\gamma$ is introduced to regulate priority difference, so the following inequality is presented.

$$
\mu_e(\boldsymbol{\xi}, \boldsymbol{c})-\mu_t(\boldsymbol{\xi}, \boldsymbol{c}) \leq \gamma, -1 \leq \gamma \leq 1 \tag{22}
$$

To facilitate adjustment of the priority relationship, variable $\delta$ is designed as an adjustment parameter for expanding the feasible domain after comprehensive optimization. Thus, there are

$$
\begin{aligned}
&\alpha^*-\delta \leq \mu_t(\boldsymbol{\xi}, \boldsymbol{c}) \leq 1 \\
&\alpha^*-\delta \leq \mu_e(\boldsymbol{\xi}, \boldsymbol{c}) \leq 1
\end{aligned} \tag{23}
$$

where $\alpha^*$ is the optimization result without considering priority.

Hence, the priority optimization model can be built as

$$
\begin{cases}
\min \gamma \\
\boldsymbol{\xi_{min}} \leq \boldsymbol{\xi} \leq \boldsymbol{\xi_{max}} \\
\boldsymbol{c_{min}} \leq \boldsymbol{c} \leq \boldsymbol{c_{max}} \\
\boldsymbol{\xi}\left(t_0\right)=\boldsymbol{\xi_0} \\
\boldsymbol{\xi}\left(t_f\right)=\boldsymbol{\xi_f} \\
\dot{\boldsymbol{\xi}}=g(\boldsymbol{\xi}, \boldsymbol{c}) \\
p\left(\boldsymbol{\xi}(1), \boldsymbol{\xi}(2), a_i, b_i, r_{xi}, r_{yi}, \omega_i, h_i\right) \geq 0, i=1, \cdots, n \\
\alpha^*-\delta \leq \mu_t(\boldsymbol{\xi}, \boldsymbol{c}) \leq 1 \\
\alpha^*-\delta \leq \mu_e(\boldsymbol{\xi}, \boldsymbol{c}) \leq 1 \\
\mu_e(\boldsymbol{\xi}, \boldsymbol{c})-\mu_t(\boldsymbol{\xi}, \boldsymbol{c}) \leq \gamma \\
-1 \leq \gamma \leq 1 \\
u_t(\boldsymbol{\xi}, \boldsymbol{c})=1-\dfrac{f_t(\boldsymbol{\xi}, \boldsymbol{c})-f_t^*}{f_t^{\max }-f_t^*} \\
u_e(\boldsymbol{\xi}, \boldsymbol{c})=1-\dfrac{f_e(\boldsymbol{\xi}, \boldsymbol{c})-f_e^*}{f_e^{\max }-f_e^*}
\end{cases} \tag{24}
$$

Although only two objectives are proposed in this paper, the idea of fuzzy satisfactory optimization is also suitable for more objective optimization.

It can be seen that the constraints include continuous differential equations in the optimization model (20) and (24). Thereby, the Gaussian pseudospectral method is introduced to transform these models into high-dimensional nonlinear programming formulations [25].

In Gaussian pseudospectral method, the Lagrangian basis function is used for discrete interpolation of state vector $\boldsymbol{\xi}$ and control vector $\boldsymbol{c}$. Further, the differential equation $\dot{\boldsymbol{\xi}}=g(\boldsymbol{\xi}, \boldsymbol{c})$ is transformed into an algebraic formulation. The terminal state $\boldsymbol{\xi}\left(t_f\right)$ is approximated to discretize the terminal constraint.

The interpolation points of the Gaussian pseudospectral method are defined in $[-1,1]$, so the time domain interval $[t_0, t_f]$ needs to be converted by the following equation

$$
s=\frac{2t-t_0-t_f}{t_f-t_0}, \ s \in [-1,1] \tag{25}
$$

The discrete points of the Gaussian pseudospectral method are $\{s_1, \cdots, s_K\}$, and the initial point $s_0 = -1$ is the $(K+1)\,th$ discrete point. The state vector and control vector can be approximated by the Lagrangian interpolation polynomials.

$$
\boldsymbol{\xi}(s) \approx \boldsymbol{\Xi}(s)=\sum_{i=0}^{K} \boldsymbol{\xi}\left(s_i\right) L_i(s) \tag{26}
$$

$$
\boldsymbol{c}(s) \approx \boldsymbol{C}(s)=\sum_{i=1}^{K} \boldsymbol{c}\left(s_i\right) L_i^*(s) \tag{27}
$$

where $\boldsymbol{\Xi}(s)$ and $\boldsymbol{C}(s)$ denote the discretized state vector and control vector, respectively. $L_i(s)$ and $L_i^*(s)$ indicate

Lagrangian interpolation polynomials as

$$L_i(s) = \prod_{j=0, j\neq i}^{K} \frac{s - s_i}{s_i - s_j}$$
$$L_i^*(s) = \prod_{j=1, j\neq i}^{K} \frac{s - s_i}{s_i - s_j}$$

Then the terminal states are approximated using discrete interpolation

$$\boldsymbol{\Xi}\left(s_f\right) = \boldsymbol{\Xi}(s_0) + \frac{t_f - t_0}{2} \sum_{k=1}^{K} \varepsilon_k g\left(\boldsymbol{\Xi}(s_k), \boldsymbol{C}(s_k)\right) \quad (28)$$

where $k = 1, \cdots, K$, $\boldsymbol{\Xi}\left(s_f\right)$ indicates the discretized terminal state, and $\varepsilon_k = \int_{-1}^{1} L_i(s)\, ds$ is the Gaussian weight.

The model constraint for each discrete point is obtained as

$$\sum_{i=0}^{K} D_i \boldsymbol{\Xi}(s_i) = \frac{t_f - t_0}{2} g\left(\boldsymbol{\Xi}(s_k), \boldsymbol{C}(s_k)\right) \quad (29)$$

$$D_i = \dot{L}_i(s_k) = \sum_{i=0}^{K} \frac{\prod_{j=0, j\neq i}^{K} s_k - s_j}{\prod_{j=0, j\neq i}^{K} s_i - s_j} \quad (30)$$

The improved P-criterion function is discretized as

$$p\left(\boldsymbol{\Xi}(1), \boldsymbol{\Xi}(2), a_i, b_i, r_{xi}, r_{yi}, \omega_i, h_i\right) \geq 0, i = 1, \cdots, n \quad (31)$$

where $\boldsymbol{\Xi}(1)$ and $\boldsymbol{\Xi}(2)$ indicate the discretized $\boldsymbol{\xi}(1)$ and $\boldsymbol{\xi}(2)$ respectively. Therefore, the discrete comprehensive optimization model can be written as

$$\begin{cases} \max \alpha \\ \boldsymbol{\xi}_{\boldsymbol{min}} \leq \boldsymbol{\Xi}(s) \leq \boldsymbol{\xi}_{\boldsymbol{max}} \\ \boldsymbol{c}_{\boldsymbol{min}} \leq \boldsymbol{C}(s) \leq \boldsymbol{c}_{\boldsymbol{max}} \\ \boldsymbol{\Xi}(s_0) = \sum_{i=0}^{K} \boldsymbol{\xi}(s_i) L_i(s_0) \\ \boldsymbol{\Xi}\left(s_f\right) = \boldsymbol{\Xi}(s_0) + \frac{t_f - t_0}{2} \sum_{k=1}^{K} \varepsilon_k g\left(\boldsymbol{\Xi}(s_k), \boldsymbol{C}(s_k)\right) \\ \sum_{i=0}^{K} D_i \boldsymbol{\Xi}(s_i) = \frac{t_f - t_0}{2} g\left(\boldsymbol{\Xi}(s_k), \boldsymbol{C}(s_k)\right) \\ p\left(\boldsymbol{\Xi}(1), \boldsymbol{\Xi}(2), a_i, b_i, r_{xi}, r_{yi}, \omega_i, h_i\right) \geq 0, i = 1, \cdots, n \\ \alpha \leq \mu_t\left(\boldsymbol{\Xi}(s), \boldsymbol{C}(s)\right) \leq 1 \\ \alpha \leq \mu_e\left(\boldsymbol{\Xi}(s), \boldsymbol{C}(s)\right) \leq 1 \\ u_t\left(\boldsymbol{\Xi}(s), \boldsymbol{C}(s)\right) = 1 - \frac{f_t\left(\boldsymbol{\Xi}(s), \boldsymbol{C}(s)\right) - f_t^*}{f_t^{\max} - f_t^*} \\ u_e\left(\boldsymbol{\Xi}(s), \boldsymbol{C}(s)\right) = 1 - \frac{f_e\left(\boldsymbol{\Xi}(s), \boldsymbol{C}(s)\right) - f_e^*}{f_e^{\max} - f_e^*} \end{cases} \quad (32)$$

The discrete priority optimization model can also be written as

$$\begin{cases} \min \gamma \\ \boldsymbol{\xi}_{\boldsymbol{min}} \leq \boldsymbol{\Xi}(s) \leq \boldsymbol{\xi}_{\boldsymbol{max}} \\ \boldsymbol{c}_{\boldsymbol{min}} \leq \boldsymbol{C}(s) \leq \boldsymbol{c}_{\boldsymbol{max}} \\ \boldsymbol{\Xi}(s_0) = \sum_{i=0}^{K} \boldsymbol{\xi}(s_i) L_i(s_0) \\ \boldsymbol{\Xi}\left(s_f\right) = \boldsymbol{\Xi}(s_0) + \frac{t_f - t_0}{2} \sum_{k=1}^{K} \varepsilon_k g\left(\boldsymbol{\Xi}(s_k), \boldsymbol{C}(s_k)\right) \\ \sum_{i=0}^{K} D_i \boldsymbol{\Xi}(s_i) = \frac{t_f - t_0}{2} g\left(\boldsymbol{\Xi}(s_k), \boldsymbol{C}(s_k)\right) \\ p\left(\boldsymbol{\Xi}(1), \boldsymbol{\Xi}(2), a_i, b_i, r_{xi}, r_{yi}, \omega_i, h_i\right) \geq 0, i = 1, \cdots, n \\ \alpha^* - \delta \leq \mu_t\left(\boldsymbol{\Xi}(s), \boldsymbol{C}(s)\right) \leq 1 \\ \alpha^* - \delta \leq \mu_e\left(\boldsymbol{\Xi}(s), \boldsymbol{C}(s)\right) \leq 1 \\ \mu_e\left(\boldsymbol{\Xi}(s), \boldsymbol{C}(s)\right) - \mu_t\left(\boldsymbol{\Xi}(s), \boldsymbol{C}(s)\right) \leq \gamma \\ -1 \leq \gamma \leq 1 \\ u_t\left(\boldsymbol{\Xi}(s), \boldsymbol{C}(s)\right) = 1 - \frac{f_t\left(\boldsymbol{\Xi}(s), \boldsymbol{C}(s)\right) - f_t^*}{f_t^{\max} - f_t^*} \\ u_e\left(\boldsymbol{\Xi}(s), \boldsymbol{C}(s)\right) = 1 - \frac{f_e\left(\boldsymbol{\Xi}(s), \boldsymbol{C}(s)\right) - f_e^*}{f_e^{\max} - f_e^*} \end{cases} \quad (33)$$

The optimal trajectory can be figured out by solving the above discrete nonlinear programming problems.

### C. TRAJECTORY TRACKING

ADRC is proposed by Han [26] to eliminate the external disturbances. It does not rely on the precise models, and shows high engineering application prospect. To reject disturbances, two first-order linear ADRC controllers are designed to follow $u_d$ and $r_d$. $v$ will converge to the desired value as well since the constraint relationship of $u, v, r$ has been established in trajectory optimization.

According to the dynamics model (5), the total disturbance $f_u$ is lumped as

$$f_u = -b_u \tau_u + \frac{1}{m_{11}} \tau_u + \frac{m_{22}}{m_{11}} vr - \frac{d_{11}}{m_{11}} u + \frac{d_X}{m_{11}} \quad (34)$$

where $b_u$ is estimation of the gain factor $1/m_{11}$. It can be seen that the total lumped disturbance consists of the internal disturbances, external disturbances, and estimation errors.

Therefore, the first equation in model (5) can be rewritten as

$$\dot{u} = b_u \tau_u + f_u \quad (35)$$

In order to estimate the longitudinal velocity and lumped disturbance, the linearly extended state observer (LESO) via (35) is designed as

$$\begin{cases} \dot{\hat{u}} = \hat{f}_u + b_u \tau_u - \beta_{u1}\left(\hat{u} - u\right) \\ \dot{\hat{f}}_u = -\beta_{u2}\left(\hat{u} - u\right) \end{cases} \quad (36)$$

where $\hat{u}$ and $\dot{\hat{u}}$ denote the estimation of the longitudinal velocity and acceleration, $\hat{f}_u$ and $\dot{\hat{f}}_u$ denote the estimation of total lumped disturbance and its differentiation. $\beta_{u1}$, $\beta_{u2}$ are two adjustable parameters of LESO for $u$.

The control law is designed by

$$\tau_u = \frac{k_u\left(u_d - \hat{u}\right) - \hat{f}_u}{b_u} \tag{37}$$

where $k_u$ is the gain.

Similarly, the following equation can be obtained from (5)

$$\dot{r} = b_r\tau_r + f_r \tag{38}$$

where $b_r$ is the estimation of the gain factor $1/m_{33}$, and $f_r$ denote the lumped disturbance.

The corresponding LESO for $r$ is designed as

$$\begin{cases} \dot{\hat{r}} = \hat{f}_r + b_r\tau_r - \beta_{r1}\left(\hat{r} - r\right) \\ \dot{\hat{f}}_r = -\beta_{r2}\left(\hat{r} - r\right) \end{cases} \tag{39}$$

where $\hat{r}$ and $\dot{\hat{r}}$ mean the estimation of the course angular velocity and acceleration. $\hat{f}_r$ and $\dot{\hat{f}}_r$ mean the estimation of total lumped disturbance and its differentiation. $\beta_{r1}$, $\beta_{r2}$ are two adjustable parameters of LESO for $r$.The control law is described as

$$\tau_r = \frac{k_r\left(r_d - \hat{r}\right) - \hat{f}_r}{b_r} \tag{40}$$

where $k_r$ is the gain. Since the tracking error of LESO can converge to zero, the closed-loop control system using these linear ADRC controllers is stable. The proof can refer to [27].

The algorithmic steps are shown in Table 2.

**TABLE 2. Algorithm steps.**

| **Algorithm 1 Control System Co-Design for USV** | |
|---|---|
| **Input:** constraints for automatic arriving and berthing of USV | |
| **Output:** $x, y, \varphi, u, v, r$ | |
| step 1 | : Establish constraints and fuzzy membership degrees |
| step 2 | : Establish the comprehensive optimization model and solve it to obtain $\alpha^*$ |
| step 3 | : Build the priority optimization model and set the initial value of $\delta$ |
| step 4 | : Solve the priority optimization model |
| step 5 | : **while** $\gamma \le 0$ |
| step 6 | : **while** the solution is satisfactory |
| step 7 | : Goto step 11 |
| step 8 | : **end while** |
| step 9 | : Increase $\delta$ and jump to step 4 |
| step 10 | : **end while** |
| step 11 | : Get desired longitudinal velocity $u_d$ and desired course angular velocity $r_d$ |
| step 12 | : Compute first-order ADRC control laws for $u_d$ and $r_d$ |
| seep 13 | : Apply the control laws to USV |

## IV. SIMULATION

Suppose the USV starts to move from (0,0) and stopping at (190,190). The constraints of state and control variables are shown in Table 3. The turning radius $k_2$ is 0.875 m. In the dynamics model of (5), the disturbances caused by wind and waves are denoted by $\boldsymbol{\tau_d} = \boldsymbol{\tau_{wind}} + \boldsymbol{\tau_{wave}} = [d_X, d_Y, d_N]^T$. $\boldsymbol{\tau_{wind}}$ denotes the wind forces and moments. It is expressed as $\boldsymbol{\tau_{wind}} = 0.5\rho_a V_r^2[C_X(\varepsilon)A_F, C_Y(\varepsilon)A_L, C_N(\varepsilon)A_L L]^T$. $V_r$ is the relative wind speed. $\rho_a$ is air density and $C_X, C_Y, C_N$ are the wind coefficients. $A_F$ and $A_L$ are the frontal and lateral projected wind areas of USV, and $L$ is the length [28]. $\boldsymbol{\tau_{wave}}$ indicates the wave-induced forces and moments, expressed as $\boldsymbol{\tau_{wave}} = 0.5\rho_w L d^2[\cos\chi D_X(\lambda_w), \sin\chi D_Y(\lambda_w), \sin\chi D_N(\lambda_w)]^T$. $\rho_w$ is water density. $d$ denotes amplitude. $\chi$ indicates encounter angle. $\lambda_w$ is wave length. $D_X, D_Y, D_N$ represents the second-order wave drift force coefficients. The parameters of the above models are time-varying and dependent on the real ocean environment. Moreover, acquiring accurate disturbance models is difficult and not necessary in this paper since verifying the proposed method's validity is the main concern. Accordingly, the disturbances of USV are replaced by the time-varying functions as $d_X = 65\cos(0.4t) + 45\sin(0.2t)$, $d_Y = 4\cos(0.2t) + 4\sin(0.6t)$, $d_N = 35\cos(0.3t) + 25\sin(0.5t)$ respectively in the following simulations [29].

**TABLE 3. The constraints of state and control variables.**

| Variable | Initial value | Terminal value | Minimum value | Maximum value |
|---|---|---|---|---|
| $x$ (m) | 0 | 190 | 0 | 200 |
| $y$ (m) | 0 | 190 | 0 | 200 |
| $\varphi$ (deg) | $45\pi/180$ | $45\pi/180$ | 0 | $90\pi/180$ |
| $u$ (m/s) | 18 | 0 | 0 | 40 |
| $v$ (m/s) | 0 | 0 | -2 | 2 |
| $r$ (deg/s) | 0 | 0 | -5 | 5 |
| $\tau_u$ (N) | | | -15000 | 18000 |
| $\tau_r$ (N*m) | | | -16000 | 15000 |

Case 1: There are four obstacles centered at (25,28), (46,65), (90,80), and (145,130).

Implement the proposed algorithm. In order to build the fuzzy membership functions of two objectives, payoff table in Table 4 is used. We can know that $f_t^* = 7.88, f_t^{\max} = 380.02$, $f_e^* = 414.9, f_e^{\max} = 382573.9$. Furthermore, the maximum membership degree is calculated as $\alpha^* = 0.8623$ by solving the comprehensive optimization model.

According to the priority optimization model, the adjustment parameter is regulated to obtain the optimization results shown in Table 5. It can be seen that all the results satisfy the optimization and priority requirement. Meanwhile, the priority deviation of these two objectives becomes larger as $\delta$ increases. The membership degree of running time increases while that of energy consumption decreases. The simulation

**TABLE 4. Payoff table for running time and energy consumption.**

| | $f_t$ | $f_e$ |
|---|---|---|
| $\min f_t(\xi, c)$ | 7.88 | 382573.9 |
| $\min f_e(\xi, c)$ | 380.02 | 414.9 |

result validates they are in conflict. Thus, a balance between objective optimization and priority is achieved. Finally, $\delta = 0.12$ is selected as the optimal trajectory.

**TABLE 5. Optimization results with different adjustment parameters.**

| $\delta$ | $\gamma$ | Target satisfaction |
|---|---|---|
| 0.03 | -0.1269 | (0.9692,0.8423) |
| 0.06 | -0.1676 | (0.9746,0.8070) |
| 0.08 | -0.1906 | (0.9764,0.7858) |
| 0.12 | -0.2389 | (0.9801,0.7412) |
| 0.15 | -0.2691 | (0.9822,0.7131) |
| 0.18 | -0.3010 | (0.9838,0.6828) |

The parameters of two ADRC controllers are shown in Table 6. The tracking results of USV are shown in the Figure 3. The obstacles are in grey, the desired path is in bule, the tracking path is in red, and the pentagram represents the target point. With the relevant constraints, the proposed algorithm computes a smooth trajectory from initial point to terminal point. It can be seen that the real trajectory effectively avoids obstacles and the USV stops exactly at the target point. Further, it is obvious that the tracking path almost coincides with the desired path.

Figure 4 shows the optimization and tracking results of $u$ and $r$. It can be seen that the real values of $u$ and $r$ precisely approach the desired values, and these two velocities converge strictly to zero when USV reaches the target point. Moreover, the absolute control errors for $u$ and $r$ are always kept within 0.1 and 0.05 respectively, which reflects the controller's good immunity against disturbances.

**TABLE 6. Parameters of ADRC controllers.**

| $b_u$ | $\beta_{u1}$ | $\beta_{u2}$ | $k_u$ |
|---|---|---|---|
| $1.3\times10^{-4}$ | $7.5\times10^{5}$ | $1.25\times10^{8}$ | 750 |
| $b_r$ | $\beta_{r1}$ | $\beta_{r2}$ | $k_r$ |
| 0.04 | $7.5\times10^{5}$ | $6.4\times10^{7}$ | 1650 |

Figure 5 shows the optimization and real results of $v$ and $\varphi$. It can be seen that their real values get closely to the desired values. The errors between them are obviously within reasonable range. The results of $\varphi$ provide further evidence that $r$ is well controlled. It should be noted that since the dynamics model is incorporated into the optimization solution, $v$ establishes a constraint relationship with $u$ and $r$. When $u$ and $r$ is precisely controlled, $v$ also converges to the desired value. The control variables are shown in Figure 6.

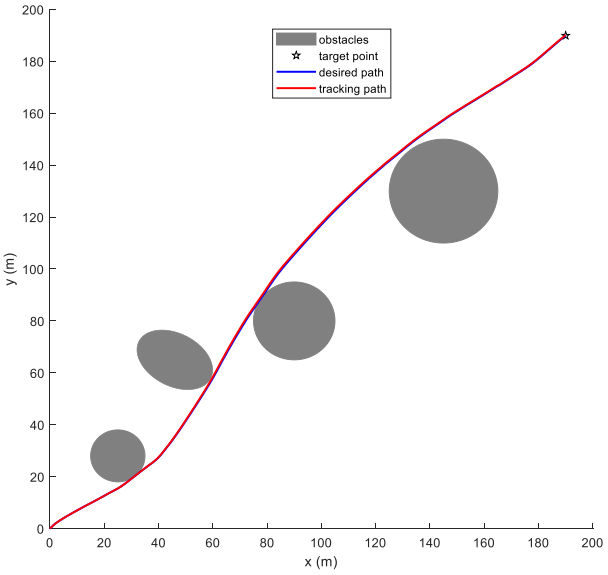


**FIGURE 3. Tracking results by the proposed algorithm in case 1.**

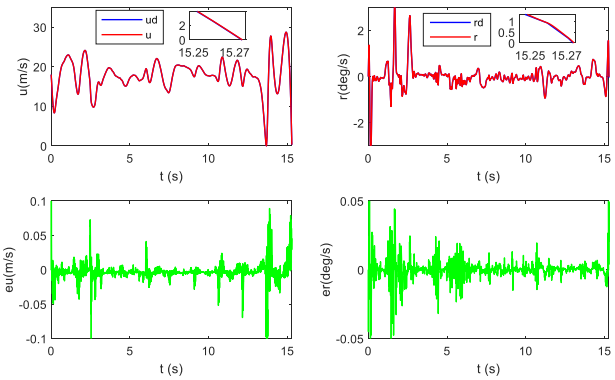


**FIGURE 4. Optimization and tracking results of $u_d$ and $r_d$ by the proposed algorithm.**

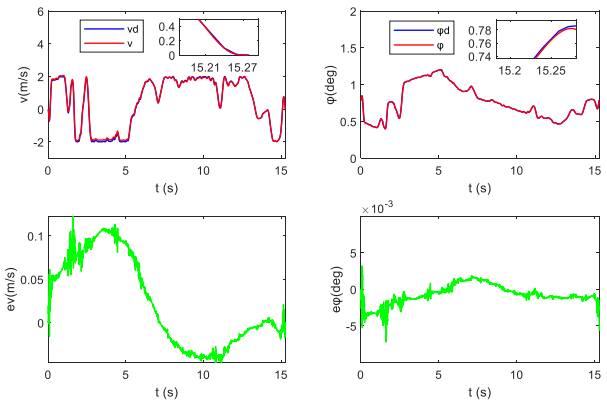


**FIGURE 5. Optimization and real results of $v$ and $\varphi$ by the proposed algorithm.**

In order to further demonstrate effectiveness of the proposed algorithm in this paper, two algorithms are carried out as comparative simulations. The first comparative method

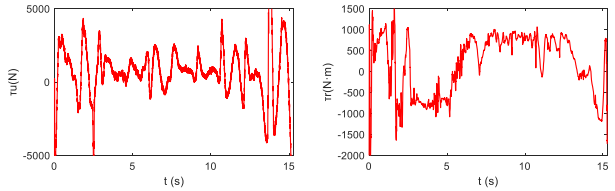


**FIGURE 6.** Control variables by the proposed algorithm.

consists of trajectory optimization based on artificial potential field (APF) and trajectory tracking based on PID control. The APF is a virtual force method proposed by Khatib, which is widely used for obstacle avoidance. It is designed based on the repulsive force field in obstacles area, and the attractive force field at target point [30]. USV avoids obstacles and reaches the target point under the two force fields. The second comparative method uses trajectory optimization by weighted multi-objective optimization (WMO) and trajectory tracking by linear quadratic regulator (LQR).

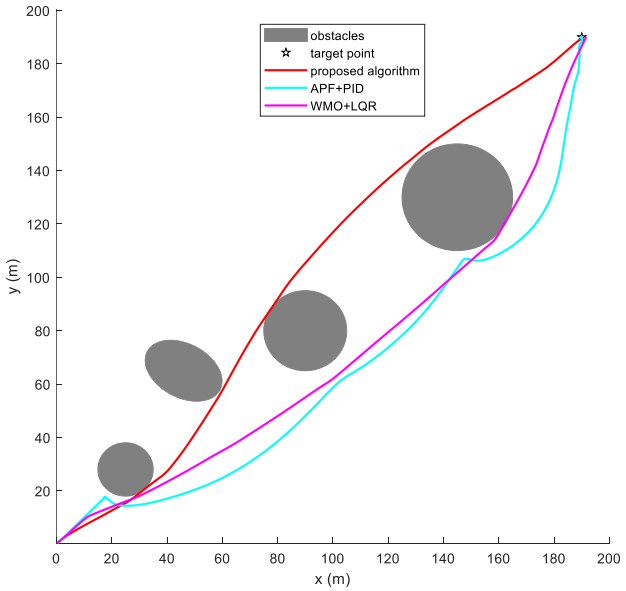


**FIGURE 7.** Tracking results by two comparative methods.

The tracking results by two comparative methods are shown in Figure 7. The grey area represents the convex obstacles and the pentagram represents the target point. The cyan curve is the result of APF+PID, and the magenta curve represents the result of WMO+LQR. Compared with the proposed algorithm, it is clear that longer distance is generated in APF+PID. Firstly, the USV travels only by attractive force in a nearly straight path in APF+PID. In the vicinity of (17.6, 17.4), the USV is subjected to the repulsive force of the first obstacle and avoids it by a combination of repulsive and attractive force. The USV is repulsed by the second obstacle at (97.6, 56.4) and its direction changes. A similar change occurs at (147.1, 106.8). It can be noticed that the USV trajectory becomes choppy while approaching the target point. In WMO+LQR, the trajectory of USV seems like a broken line. It is obvious that two irrational turns happen at (11.5,10.4) and (158.7,114.3), which does not conform to the actual navigation of USV. Due to the poor disturbance rejection of LQR, the USV does not reach the target point accurately but stops at (191.5,189.7).

**TABLE 7.** Comparison of optimization objectives.

| | The proposed algorithm | APF+PID | WMO+LQR |
|---|---|---|---|
| running time | 15.27 | 118.62 | 14.41 |
| energy consumption | $9.83\times10^4$ | $3.11\times10^4$ | $1.67\times10^5$ |

As shown in Table 7, running time in the proposed algorithm is 15.27 and energy consumption is $9.83 \times 10^4$, by which a good balance between the two objectives is achieved. In APF+ PID, running time is 118.62 and energy consumption is $3.11 \times 10^4$. The APF method only considers obstacle avoidance. It takes too much time and is not acceptable in real sailing. In WMO+LQR, running time is 14.41, similar to the proposed algorithm. However, it consumes almost twice energies as much as the proposed algorithm. This shows that fuzzy optimization is better than weighted optimization.

Figure 8 shows the optimization and tracking results of $u$ and $r$ by APF+PID. The attractive force is smaller when the USV is closer to the target. Therefore, the velocities of USV become extremely low when approaching the target position. Figure 9 shows the transverse velocity, course angle and control variables.

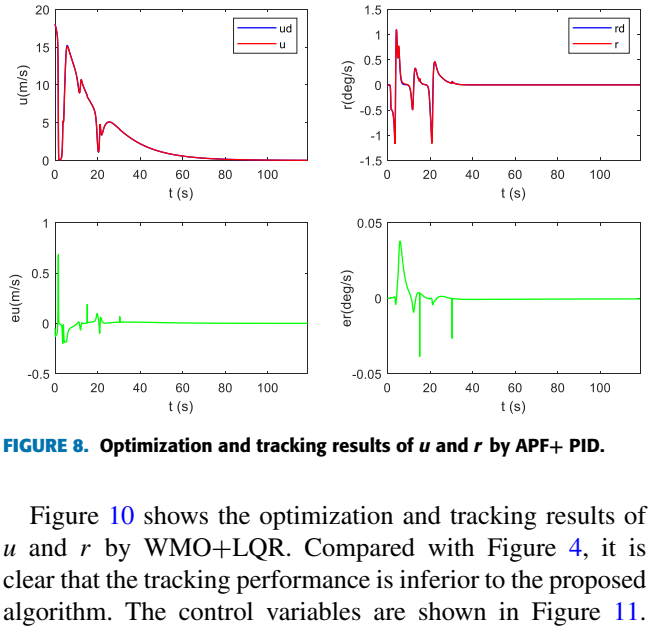


**FIGURE 8.** Optimization and tracking results of $u$ and $r$ by APF+ PID.

Figure 10 shows the optimization and tracking results of $u$ and $r$ by WMO+LQR. Compared with Figure 4, it is clear that the tracking performance is inferior to the proposed algorithm. The control variables are shown in Figure 11. They are both larger than the proposed method so that energy consumption increases.

Case 2: There are four obstacles centered at (45,45), (70,110), (105,80), and (130,140). Other conditions are the same as in Case 1.

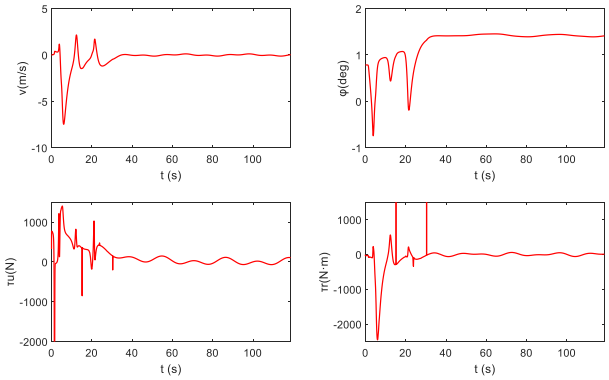


**FIGURE 9.** Transverse velocity, course angle and control variables by APF+PID.

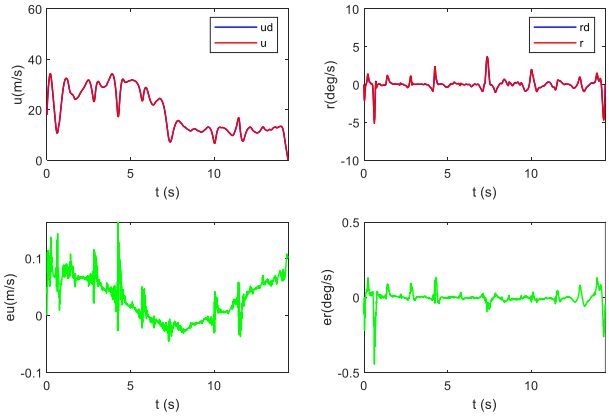


**FIGURE 10.** Optimization and tracking results of $u$ and $r$ by WMO+LQR.

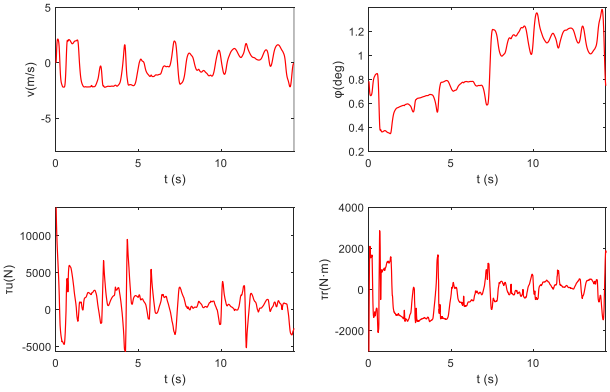


**FIGURE 11.** Transverse velocity, course angle and control variables by WMO+LQR.

The tracking results are shown in the Figure 12. It can be seen that the proposed method is still able to compute an optimal trajectory when the positions and orientation of the obstacles change. Moreover, USV is able to track the trajectory with high accuracy. Running time is 14.79 and energy consumption is $1.21 \times 10^5$.

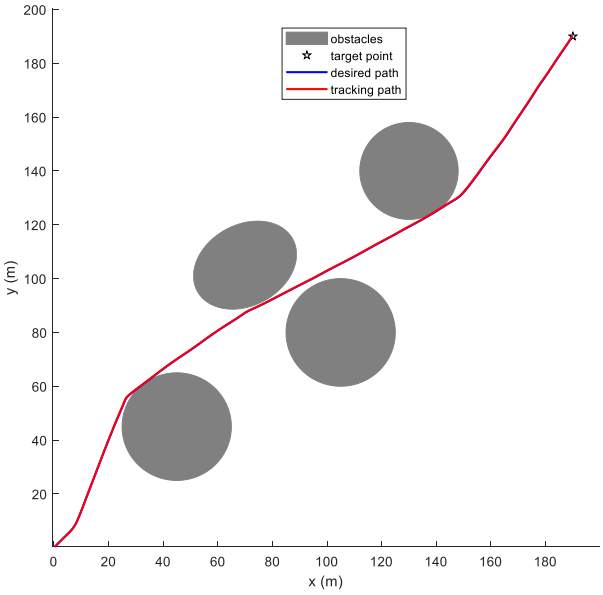


**FIGURE 12.** Tracking results by the proposed algorithm in case 2.

## V. CONCLUSION

This paper proposes a co-design method of control system to accomplish the task of automatic target arriving and berthing for USV. For trajectory optimization, fuzzy satisfactory optimization is adopted and fuzzy membership degree difference is used to model priority. The model constraint includes both kinematic and dynamic models. Moreover, the obstacle avoidance constraint is designed based on the improved P-criterion. The comprehensive optimization model and priority optimization model are built such that balance between optimization and priority can be realized by relaxing the maximum membership degree. By using the Gaussian pseudospectral method, the continuous differential constraint is converted into discrete algebra constraint. The optimal trajectory is obtained by solving these two models. For trajectory tracking, the longitudinal velocity and course angular velocity are respectively steered by two first-order linear ADRC controllers. Such a design can reduce feedback cost and facilitate controller design. The simulation proves that the system is able to accomplish the task of automatic target arriving and berthing in presence of multi-shape convex obstacles and disturbances. In the future, motion obstacles will be concerned in trajectory optimization and tracking of USV.

## APPENDIX

## GLOSSARY

| | |
|---|---|
| USV | unmanned surface vehicle. |
| ADRC | active disturbance rejection control. |
| LG | Legendre Gaussian. |
| $u$ | longitudinal velocity. |
| $v$ | transverse velocity. |
| $r$ | course angular velocity. |

| | |
|---|---|
| $\varphi$ | course angle. |
| $\boldsymbol{\tau}$ | surge force and yaw moments. |
| $\boldsymbol{\tau_d}$ | external disturbances. |
| $\boldsymbol{M}$ | inertial matrix. |
| $\boldsymbol{C}$ | Coriolis matrix. |
| $\boldsymbol{D}$ | hydrodynamic damping matrix. |
| $\boldsymbol{\xi}$ | state vector. |
| $\boldsymbol{c}$ | control vector. |
| $r_x$ | proportional coefficient in the x-direction. |
| $r_y$ | proportional coefficient in the y-direction. |
| $(a, b)$ | coordinates of the obstacle's center. |
| $h$ | adjustable parameter for obstacle shape. |
| $\omega$ | obstacle's orientation angle. |
| $n$ | number of obstacles. |
| $k_2$ | turning radius. |
| $\alpha^*$ | maximum membership degree. |
| $\gamma$ | priority difference. |
| $\delta$ | adjustment parameter. |
| $f_u$ | lumped disturbance for $u$. |
| $b_u$ | estimation of the gain factor $1/m_{11}$. |
| $f_r$ | lumped disturbance for $r$. |
| $b_r$ | estimation of the gain factor $1/m_{33}$. |
| $\boldsymbol{\tau_{wind}}$ | wind forces and moments. |
| $\boldsymbol{\tau_{wave}}$ | wave forces and moments. |
| $V_r$ | relative wind speed. |
| $\rho_a$ | air density. |
| $\rho_w$ | water density. |
| LESO | linearly extended state observer. |
| APF | artificial potential field. |
| LQR | linear quadratic regulator. |
| WMO | weighted multi-objective optimization. |

## REFERENCES


[1] S. Yuan, Z. Liu, Y. Sun, Z. Wang, and L. Zheng, "An event-triggered trajectory planning and tracking scheme for automatic berthing of unmanned surface vessel," *Ocean Eng.*, vol. 273, Apr. 2023, Art. no. 113964.

[2] S. Han, L. Wang, and Y. Wang, "A potential field-based trajectory planning and tracking approach for automatic berthing and COLREGs-compliant collision avoidance," *Ocean Eng.*, vol. 266, Dec. 2022, Art. no. 112877.

[3] J. Liu, H. Chen, S. Xie, Y. Peng, D. Zhang, and H. Pu, "Trajectory planning for unmanned surface vehicles in multi-ship encounter situations," *Ocean Eng.*, vol. 285, Oct. 2023, Art. no. 115384.

[4] C. Wu, W. Yu, W. Liao, and Y. Ou, "Deep reinforcement learning with intrinsic curiosity module based trajectory tracking control for USV," *Ocean Eng.*, vol. 308, Sep. 2024, Art. no. 118342.

[5] T. Huang, Z. Xue, Z. Chen, and Y. Liu, "Efficient trajectory planning and control for USV with vessel dynamics and differential flatness," in *Proc. IEEE/ASME Int. Conf. Adv. Intell. Mechatronics (AIM)*, Seattle, WA, USA, Jun. 2023, pp. 1273–1280.

[6] L. Zhao, Y. Bai, and J. K. Paik, "Global–local hierarchical path planning scheme for unmanned surface vehicles under dynamically unforeseen environments," *Ocean Eng.*, vol. 280, Jul. 2023, Art. no. 114750.

[7] M. K. Nutalapati, A. S. Bedi, K. Rajawat, and M. Coupechoux, "Online trajectory optimization using inexact gradient feedback for time-varying environments," *IEEE Trans. Signal Process.*, vol. 68, pp. 4824–4838, 2020.

[8] A. B. Mills, D. Kim, and E. W. Frew, "Energy-aware aircraft trajectory generation using pseudospectral methods with differential flatness," in *Proc. IEEE Conf. Control Technol. Appl. (CCTA)*, Aug. 2017, pp. 1536–1541.

[9] X. Wang, Z. Deng, H. Peng, L. Wang, Y. Wang, L. Tao, C. Lu, and Z. Peng, "Autonomous docking trajectory optimization for unmanned surface vehicle: A hierarchical method," *Ocean Eng.*, vol. 279, Jul. 2023, Art. no. 114156.

[10] A. Kandel, C. Xu, D. Cardona, and C. Whitehair, "Fuel and time optimal USV trajectory planning under flexible refueling constraints," 2020, *arXiv:2011.03097*.

[11] J. Dong, M. Zhao, M. Cheng, and Y. Wang, "Integral terminal sliding-mode integral backstepping adaptive control for trajectory tracking of unmanned surface vehicle," *Cyber-Physical Syst.*, vol. 9, no. 1, pp. 77–96, Jan. 2023.

[12] Z. Dong, L. Wan, Y. Li, T. Liu, and G. Zhang, "Trajectory tracking control of underactuated USV based on modified backstepping approach," *Int. J. Nav. Archit. Ocean Eng.*, vol. 7, no. 5, pp. 817–832, Sep. 2015.

[13] C. Yu, J. Zhu, Y. Hu, H. Zhu, N. Wang, H. Guo, Q. Zhang, and S. Liu, "Prescribed-time observer-based sideslip compensation in USV line-of-sight guidance," *Ocean Eng.*, vol. 298, Apr. 2024, Art. no. 117177.

[14] Y. Fan, B. Qiu, L. Liu, and Y. Yang, "Global fixed-time trajectory tracking control of underactuated USV based on fixed-time extended state observer," *ISA Trans.*, vol. 132, pp. 267–277, Jan. 2023.

[15] X.-N. Yu, L.-Y. Hao, and X.-L. Wang, "Fault tolerant control for an unmanned surface vessel based on integral sliding mode state feedback control," *Int. J. Control, Autom. Syst.*, vol. 20, no. 8, pp. 2514–2522, Aug. 2022.

[16] Y. Yao, J.-H. Cao, Y. Guo, Z. Fan, B. Li, B. Xu, and K. Li, "Adaptive coverage control for multi-USV system in complex environment with unknown obstacles," *Int. J. Distrib. Sensor Netw.*, vol. 17, no. 6, Jun. 2021, Art. no. 155014772110215.

[17] J. Ning, Y. Ma, T. Li, C. L. P. Chen, and S. Tong, "Event-triggered based trajectory tracking control of under-actuated unmanned surface vehicle with state and input quantization," *IEEE Trans. Intell. Vehicles*, vol. 9, no. 2, pp. 3127–3139, Feb. 2024.

[18] N. Wang, Z. Liu, Z. Zheng, and M. J. Er, "Global exponential trajectory tracking control of underactuated surface vehicles using dynamic surface control approach," in *Proc. Int. Conf. Intell. Auto. Syst. (ICoIAS)*, Singapore, Mar. 2018, pp. 221–226.

[19] B. Zhou, B. Huang, Y. Su, Y. Zheng, and S. Zheng, "Fixed-time neural network trajectory tracking control for underactuated surface vessels," *Ocean Eng.*, vol. 236, Sep. 2021, Art. no. 109416.

[20] M. J. Er and Z. Li, "Formation control of unmanned surface vehicles using fixed-time non-singular terminal sliding mode strategy," *J. Mar. Sci. Eng.*, vol. 10, no. 9, p. 1308, Sep. 2022.

[21] S. Li and C. Hu, "Two-step interactive satisfactory method for fuzzy multiple objective optimization with preemptive priorities," *IEEE Trans. Fuzzy Syst.*, vol. 15, no. 3, pp. 417–425, Jun. 2007.

[22] J. Witt and M. Dunbabin, "Go with the flow: Optimal AUV path planning in coastal environments," in *Proc. Austral. Conf. Robot. Automat.*, Canberra, ACT, Australia, Dec. 2008, pp. 1–9.

[23] T. Gu, "Improved trajectory planning for on-road self-driving vehicles via combined graph search, optimization & topology analysis," Ph.D. dissertation, Dept. Elect. Comput. Eng., Carnegie Mellon Univ., Pittsburgh, PA, USA, 2017.

[24] D. Jones and G. A. Hollinger, "Planning energy-efficient trajectories in strong disturbances," *IEEE Robot. Autom. Lett.*, vol. 2, no. 4, pp. 2080–2087, Oct. 2017.

[25] Q. Hu, P. Liu, and J. Yang, "Improved Gauss pseudospectral method for UAV trajectory planning with terminal position constraints," *J. Inf. Process. Syst.*, vol. 19, no. 5, pp. 563–575, Oct. 2023.

[26] J. Han, *The Technique for Estimating and Compensating the Uncertainties: Active Disturbance Rejection Control Technique*. Beijing, China: National Defense Industry Press, 2008.

[27] Z.-Q. Chen, M.-W. Sun, and R.-G. Yang, "On the stability of linear active disturbance rejection control," *Acta Automatica Sinica*, vol. 39, no. 5, pp. 574–580, Mar. 2014.

[28] T. I. Fossen, "How to incorporate wind, waves and ocean currents in the marine craft equations of motion," in *Proc. 9th IFAC*, Arenzano, Italy, Sep. 2012, pp. 126–131.

[29] Y. Wang, C. Liu, and K. Xie, "Finite time tracking control for USV with external disturbance," in *Proc. China Autom. Congr. (CAC)*, Beijing, China, Oct. 2021, pp. 2969–2974.

[30] G. Zhang, J. Han, J. Li, and X. Zhang, "APF-based intelligent navigation approach for USV in presence of mixed potential directions: Guidance and control design," *Ocean Eng.*, vol. 260, Sep. 2022, Art. no. 111972.

**TAOYI CHEN** received the M.S. and Ph.D. degrees in electrical engineering from Harbin Institute of Technology, China, in 2008 and 2012, respectively. Currently, he is a Professor with The 54th Research Institute, China Electronics Technology Group Corporation. He has published a great deal of papers in journals and conferences. His research interests include unmanned autonomous systems, guidance and control, big data mining, and remote sensing image processing.

**HUIXIANG PENG** received the B.S. degree in industrial automation from Hebei University of Technology, China, in 1997, and the M.S. degree in computer application from Xidian University, China, in 2009. He is currently with The 54th Research Institute, China Electronics Technology Group Corporation, as a Professor. His research interests include optimal control, remote sensing image processing, and intelligent spatial information processing.

**XIAOYU CHANG** received the B.S. degree in surveying and mapping engineering from Southeast University, Nanjing, China, in 2017, and the M.S. degree in photogrammetry and remote sensing from Wuhan University, Wuhan, China, in 2020. During the master's degree, he has published three high-level articles, mainly related to remote sensing image processing, semi-supervised learning, and dataset preparation. Currently, he is with The 54th Research Institute, China Electronics Technology Group Corporation, as an Engineer. His research interests include UAV visual positioning, remote sensing image processing, remote sensing target recognition, and satellite positioning. During his work, he has also published five articles and authorized eight patents.

**XIAONAN ZHANG** received the B.S. degree from Harbin Engineering University, Harbin, China, in 2016, and the M.S. degree from the University of Chinese Academy of Sciences, Changchun, China, in 2019. He is currently an Engineer with The 54th Research Institute, China Electronics Technology Group Corporation. His research interests include the object detection and remote sensing image interpretation.

**DIDI WANG** received the B.S. degree from Tianjin University, China, in 2022, where he is currently pursuing the M.S. degree with the School of Electrical and Information Engineering. His research interests include active disturbance rejection control, trajectory optimization and tracking, UAV formation, and deep learning. In addition, he works on formation of unmanned aerial vehicle and unmanned surface vehicle.